ELSEVIER

Contents lists available at ScienceDirect

Computers in Biology and Medicine

journal homepage: www.elsevier.com/locate/compbiomed



Unsupervised neural decoding for concurrent and continuous multi-finger force prediction

Long Meng ^a, Xiaogang Hu ^{a,b,c,d,e,*}

- ^a Department of Mechanical Engineering, Pennsylvania State University-University Park, PA, USA
- ^b Department of Kinesiology, Pennsylvania State University-University Park, PA, USA
- ^c Department of Physical Medicine & Rehabilitation, Pennsylvania State Hershey College of Medicine, PA, USA
- ^d Huck Institutes of the Life Sciences, Pennsylvania State University-University Park, PA, USA
- e Center for Neural Engineering, Pennsylvania State University-University Park, PA, USA

ARTICLE INFO

Keywords: Unsupervised neural decoding Hand function Finger force prediction Machine learning Biosignal processing

ABSTRACT

Reliable prediction of multi-finger forces is crucial for neural-machine interfaces. Various neural decoding methods have progressed substantially for accurate motor output predictions. However, most neural decoding methods are performed in a supervised manner, i.e., the finger forces are needed for model training, which may not be suitable in certain contexts, especially in scenarios involving individuals with an arm amputation. To address this issue, we developed an unsupervised neural decoding approach to predict multi-finger forces using spinal motoneuron firing information. We acquired high-density surface electromyogram (sEMG) signals of the finger extensor muscle when subjects performed single-finger and multi-finger tasks of isometric extensions. We first extracted motor units (MUs) from sEMG signals of the single-finger tasks. Because of inevitable finger muscle co-activation, MUs controlling the non-targeted fingers can also be recruited. To ensure an accurate finger force prediction, these MUs need to be teased out. To this end, we clustered the decomposed MUs based on inter-MU distances measured by the dynamic time warping technique, and we then labeled the MUs using the mean firing rate or the firing rate phase amplitude. We merged the clustered MUs related to the same target finger and assigned weights based on the consistency of the MUs being retained. As a result, compared with the supervised neural decoding approach and the conventional sEMG amplitude approach, our new approach can achieve a higher R^2 (0.77 \pm 0.036 vs. 0.71 \pm 0.11 vs. 0.61 \pm 0.09) and a lower root mean square error (5.16 \pm 0.58 % MVC vs. 5.88 \pm 1.34 %MVC vs. 7.56 \pm 1.60 %MVC). Our findings can pave the way for the development of accurate and robust neural-machine interfaces, which can significantly enhance the experience during humanrobotic hand interactions in diverse contexts.

1. Introduction

Human hands exhibit remarkable dexterity, allowing us to perform a variety of motions with high precision. With the rapid advancements in robotics, cutting-edge prosthetics, and exoskeletal hands can now actuate individual fingers or even joints [1], approaching the proficiency of the human hand. To maximize the potential of these sophisticated robotic systems in rehabilitation, assistance, or remote operations, it is crucial to develop accurate and robust neural-machine interfaces for intuitive interactions between humans and robots [2]. It is possible to derive neural command signals from various sources such as the brain [3], peripheral nerves [4], and muscles [5]. These physiological signals can be interpreted for motion intention recognition, and

these signals can further be translated into directives to facilitate interaction with advanced robotic systems [6,7]. However, accurate decoding of individual finger motor output remains a challenge for reliable and dexterous neural-machine interactions.

Recent progress has seen the advent of brain-machine interfaces (BMIs) leveraging state-based decoding techniques [8–11]. Such decoders are pivotal for enhancing the performance of BMIs by distinguishing different brain states related to hand movements. For example, Aggarwal et al. [8] combined local field potential (LFP)-based state decoding with spike-based kinematic decoding to enhance the accuracy of reach-to-grasp movements. Ahmadi et al. [9] applied the common spatial pattern (CSP) algorithm on various spectral LFP sub-bands to improve the distinction between two classes: force and rest.

https://doi.org/10.1016/j.compbiomed.2024.108384

Received 21 October 2023; Received in revised form 27 February 2024; Accepted 24 March 2024 Available online 27 March 2024 0010-4825/© 2024 Elsevier Ltd. All rights reserved.

^{*} Corresponding author. Pennsylvania State University-University Park, 205 Reber Building, University Park, PA, 16802, USA. *E-mail address:* xxh120@psu.edu (X. Hu).

In addition, they found that combining discrete state decoders with continuous force decoders could improve force decoding performance. Farrokhi et al. [10] introduced a state-based probabilistic approach to decode hand positions from ECoG signals in Rhesus monkeys during unilateral and bilateral movements. Although promising, two challenges need to be tackled for practical implementation: 1) These studies relied on invasive methods, necessitating surgical implantation of electrodes, which raised concerns regarding human user adoptions. 2) The studies were conducted on animal models, necessitating further validation to ensure safety, effectiveness, and reliability in human applications. Correspondingly, recent developments in non-invasive BMIs present a promising alternative. For example, Hosseini et al. [11] recorded electroencephalogram (EEG) data in a non-invasive manner. In this study, a binary discrete decoder was built to detect the axis of movements using CSP features. Along each axis, a non-parametric continuous decoder was trained using the envelope features of EEG data to conduct an accurate and continuous hand movement decoding. However, the process of acquiring EEG data remains cumbersome. These issues encompass aspects such as setup time and complexity, wearability and comfort, mobility restrictions, and user acceptance. Additionally, the typical low signal-to-noise ratio of scalp EEG complicates the differentiation of various brain activities [12]. In light of these difficulties, the exploration of alternative methods for capturing neural signals in a relatively easy way has become increasingly pertinent. In this context, surface electromyogram (sEMG) emerges as a compelling option.

sEMG, a type of non-invasive neural signal obtained from the skin surface [13], is formed as a summation of hundreds of motor unit action potentials (MUAPs) stemming from motor unit (MU) discharges. The number of MUAPs in a given time tends to scale with the level of descending neural drive signal to the muscles, it is therefore feasible to decode motion intentions using sEMG signals, which has gained significant attention in the field of neural-machine interfaces partly due to its non-invasive nature [14-16]. Regarding decoding techniques, pattern recognition approaches [17-20] have advanced substantially to identify numerous hand movements [21]. However, these approaches can only recognize pre-defined motions, and these motions cannot be recognized in a continuous way. As an alternative approach, proportional direct control continuously maps or converts sEMG features to the desired motor output using regression-based approaches [15,22]. Direct control allows users to conduct continuous control of a single degree of freedom by varying sEMG features, which can generally be categorized as macroscopic features and microscopic features. The macroscopic features (such as sEMG amplitude) are extracted directly from global sEMG signals, which have been widely adopted in myoelectric control [21]. However, the advancement of continuous finger motion prediction using global sEMG features is constrained due to several issues [19,20], including crosstalk arising from neighboring muscles or muscle compartments [23], inconsistent electrode placement over time, and biased sEMG recording caused by various interferences, such as superimposition of MUAPs, motion artifact, and background noise. These factors can lead to overestimation or underestimation errors, thereby degrading the decoding performance.

In contrast, with the advent of flexible high-density sEMG (HD-sEMG) electrode array techniques, it is now possible to perform neuro-muscular information analysis from the microscopic perspective (via motoneuron discharge trains extracted from HD-sEMG signals) [24]. Firing event trains can be employed for motor output predictions. To be specific, the spinal motoneurons receive excitatory neural drive from the brain. Then, the neural drive is transformed into MU firing event trains. The population discharge frequency of MUs can be employed to indicate the neural drive and further be used to predict motor output. Previous studies [25–28] have developed a neural decoding-based approach and have demonstrated the superiority of concurrently predicting finger forces using motoneuron discharge information. Prior to finger force predictions, because of the inevitable MU recruitment of untargeted fingers, measure finger forces were used to refine the MU pool based on

the correlation between finger forces and MU firing rate. This supervised approach might not be feasible in some cases, such as scenarios involving individuals with hand disabilities. For example, individuals with hand amputation do not allow finger force measurement, and individuals with a brain injury may not be able to voluntarily exert well-controlled forces on their individual fingers, making finger force measurements unfeasible. Therefore, there is a need to develop an unsupervised approach that can bypass the need for direct force measurements, which is the focus of the current study. Such an approach can offer a more inclusive and adaptable solution for a wider range of users, including those with hand impairments.

In our study, each participant performed two types of tasks (i.e., single-finger tasks for MU extraction, and multi-finger tasks for the MU weight assignment and decoder performance evaluation). Previous studies revealed that a relatively large enslaving was observed between the ring and little fingers [29-31]. Based on the sEMG recordings, similar activation patterns can be found for the EDC muscle compartments of the ring and little fingers [32]. Consequently, the ring and little fingers were required to extend simultaneously, and the forces were aggregated for subsequent analyses [28]. As illustrated in Fig. 1, we first decomposed sEMG signals of single-finger tasks. Due to inevitable finger muscle co-activation, MUs related to non-targeted fingers may also be recruited. Those MUs should be excluded for accurate force prediction. Therefore, we conducted a MU clustering and labeling procedure to exclude MUs not associated with target fingers. We assigned weights to MUs based on the consistency of the MUs being retained across multi-finger trials. We found that our developed decoder model outperformed existing state-of-the-art neural decoders with a higher force prediction accuracy. Our unsupervised approach can broaden the applicability of the neural decoding techniques. The outcomes also hold potential benefits for a more intuitive experience during human-machine interactions.

2. Methods

2.1. Experimental data acquisition and preprocessing

Eight subjects (1 female and 7 males) were employed for the

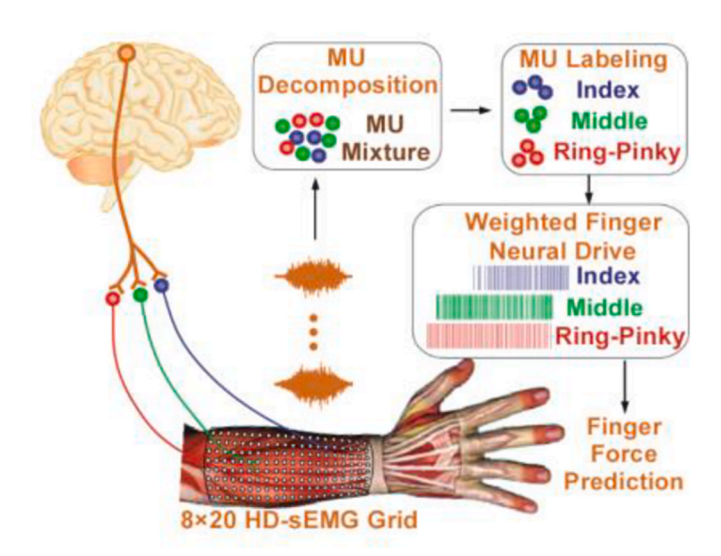


Fig. 1. Overview of the research framework. The brain sends neural drive to different sub-groups of motoneurons innervating different finger extensor compartments. We extract the MU pool containing a mixture of MUs of different fingers from HD-sEMG recordings. We then perform unsupervised neural decoding procedures (MU clustering, labeling, and weight assignment) to derive the weighted neural drive signals for individual fingers, which can be used for continuous force predictions.

experiment. All subjects were aged between 21 and 35 years without any known neurological or muscular disorders. Before participation, subjects signed the informed consent to acknowledge that they fully understood the research purposes, their rights, and potential risks. The study protocol was approved by the Institutional Review Board of the Pennsylvania State University (Approval Number: STUDY00021035).

As for the experimental setup, subjects were allowed to adjust the height of the seating chair to their preferred comfort level. The forearm rested on the table in a neutral position, and the wrist was restricted in a neutral state to minimize finger force contamination. Four fingers (index, middle, ring, and little fingers) were involved in this study. To track the extension force of each finger, we separately secured four fingers to four miniature load cells (SM-200 N, Interface). The measured forces were displayed to subjects in real time as visual feedback and were acquired at a sampling frequency of 1000 Hz. The corresponding sEMG data were measured with an 8 × 20 high-density electrode array (diameter of electrode: 3 mm, inter-electrode distance: 10 mm) attached over the extensor digitorum communis (EDC) muscle, as shown in Fig. 1. The covering area of the electrode array was determined by palpating the EDC muscles at the time of finger extensions. The monopolar sEMG signals were recorded using the EMG-USB2+ (OT Bioelettronica, Torino, Italy), with a gain of 1000, a pass band of 10–900 Hz, and a sampling frequency of 2048 Hz. Then, an independent component analysis (ICA)based interference detection and removal approach was adopted to eliminate the motion artifacts with minimal distortion of the sEMG signals [33]. This approach could effectively remove power line noise and motion artifacts. First, sEMG signals were decomposed into independent components using the Infomax ICA algorithm. Second, for each separated component, power line noise was detected using spectral analysis and mitigated through notch filtering. Motion artifacts were addressed by a high-pass filter and peak thresholding techniques. Refer to Section A in the Supplementary Material for the detailed techniques of interference removal. The final step aimed to reconstruct the sEMG signals from the processed components. The denoised sEMG signals $\widetilde{x} = \mathbf{W}^{-1}\widetilde{\epsilon}$, where \mathbf{W}^{-1} denotes the original mixing matrix obtained from the ICA process, $\widetilde{\epsilon}$ denotes the processed components. This approach can effectively reduce noise artifacts (as shown in Fig. 2), thereby enhancing the signal quality for further analysis.

At the beginning of the experiment, we measured the maximum voluntary contraction (MVC) force of each involved finger when subjects performed the maximum isometric extension of the related fingers. During the main experiment, subjects were required to perform two types of isometric extension tasks, termed single-finger task and multifinger task, respectively. For the single-finger task, only one single finger (ring and little fingers were treated as one finger) was active for each trial, as shown in Fig. 3(a). Subjects followed a 21-s trapezoid force target trajectory using their target finger, with instructions to minimize the co-activation of other non-targeted fingers. Fifteen single-finger trials (3 fingers \times 5 trials/finger) in total were performed. For the multi-finger task, we randomly selected at least two fingers for each trial. Each target finger took turns to follow a trapezoid force trajectory with 1-s duration of rest between trajectories, as shown in Fig. 3(b) and (c). The duration of each trial was 36 s for the three-finger combination and 12 s for the two-finger combinations. Twenty-eight multi-finger trials in total were performed. Because we aimed to evaluate the multifinger force prediction for dexterous control of assistive robots, cocontractions of other non-targeted fingers were allowed during the multi-finger task.

2.2. Unsupervised neural decoding using firing rate information

As shown in Fig. 4, the overall approach included four steps: 1. Initial MU extraction, 2. MU clustering, 3. MU weight assignment, and 4. Force prediction performance evaluation. Briefly, we first extracted MUs using

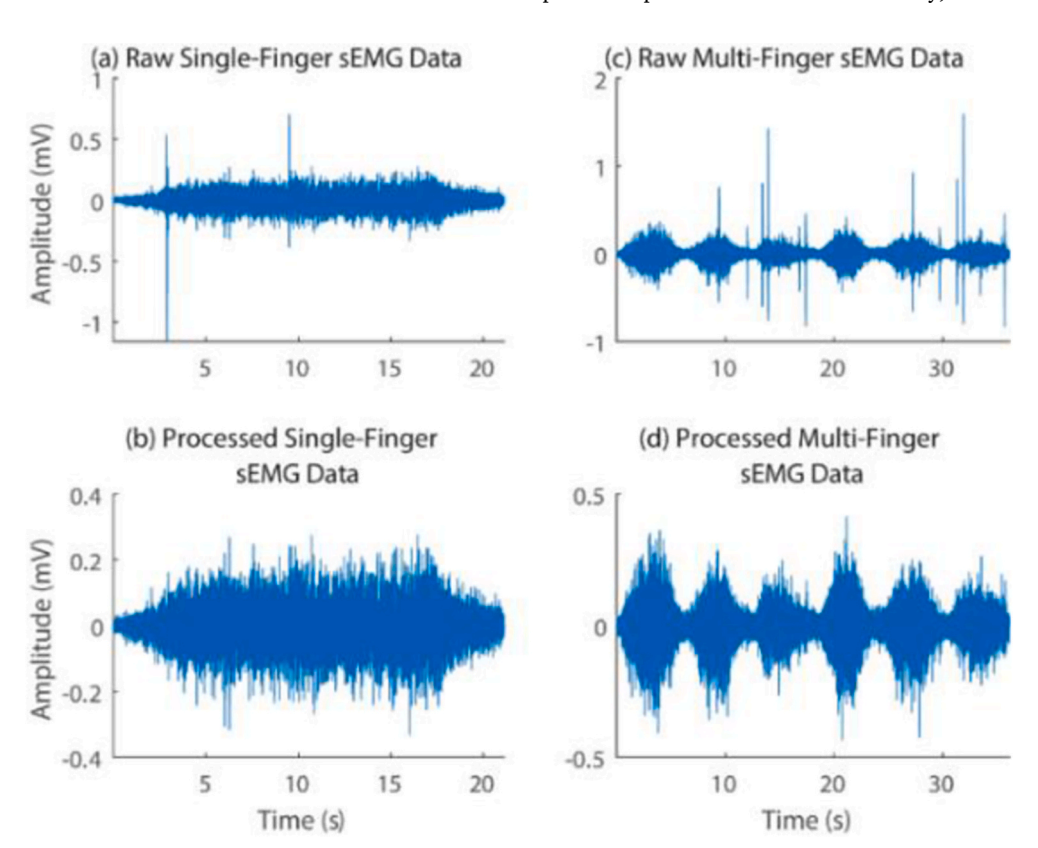


Fig. 2. Examples of the single-finger and multi-finger sEMG data before and after ICA-based interference detection and removal approach. (a) and (b) show a representative single-finger sEMG signal before and after artifact removal, respectively. (c) and (d) show a representative multi-finger sEMG signal before and after artifact removal, respectively.

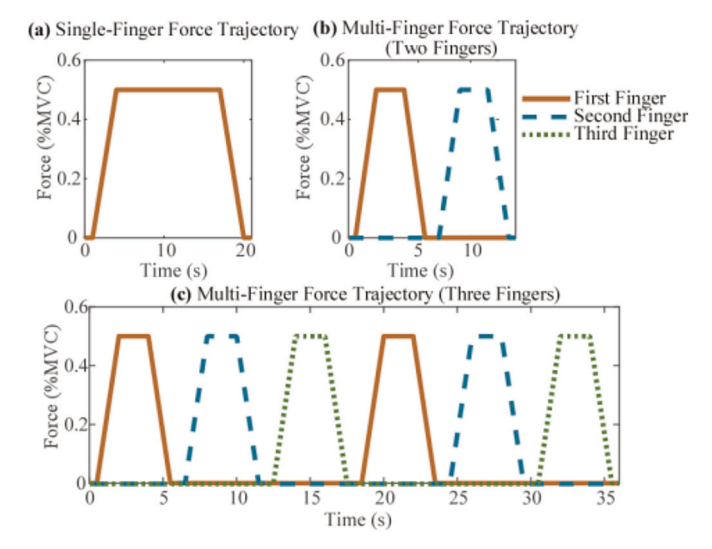


Fig. 3. Designed force trajectories. (a) A 21-s trapezoid force target trajectory for a single-finger task, where subjects were instructed to minimize coactivation of non-targeted fingers. (b) and (c) Trapezoid force trajectories for multi-finger tasks, with each target finger following the trajectory in succession and a 1-s rest between trajectories. The total trial duration was 12 s for two-finger combinations and 36 s for three-finger combinations. In the multi-finger tasks, co-contractions were permitted to assess the force prediction capabilities for each finger combination.

the sEMG data of single-finger trials. We then clustered and labeled the extracted MUs based on the shape similarity of the firing rate profiles over time. For a fair comparison, we adopted a four-fold cross-validation approach to avoid in-sample optimization bias by dividing the multi-

finger trials into the refinement dataset (i.e., three folds for MU weight assignment) and testing dataset (i.e., one fold for model evaluation using the weighted MU sets).

2.2.1. MU extraction

We decomposed the HD-sEMG signals obtained during single-finger tasks via the fast independent component analysis (FastICA) algorithm [34], which has been widely used in recent studies [19,20,35–37] for the blind source separation due to its relatively high computational efficiency. As shown in Fig. 5, after artifact removal, we first selected 60 channels with maximum root mean square (RMS) values from 160 channels for subsequent decomposition. By taking this step, we can decrease the computational cost and exclude channels contributing little to the decomposition accuracy [19,20]. Then, we conducted the channel extension procedure by a factor of 10 to increase the number of observations and whitened the extended sEMG data to remove the correlation between observations. Lastly, we applied the FastICA algorithm to decompose the whitened sEMG signals. Refer to Section B in the Supplementary Material for the procedures of FastICA-based sEMG decomposition. Because subjects were required to perform a single-finger task using the same finger multiple times, we pooled the decomposed MUs from the same finger together to form the Raw MU Set for this finger. Correspondingly, the separation matrixes obtained using different single-finger trials were concatenated to form $B_{0,l}$. Duplicate MUs were then removed in subsequent steps.

2.2.2. MU clustering and labeling

Despite instructions for subjects to isolate force output to a single finger, co-activations of other fingers were inevitable, due to the finger enslavement effect [29–31]. As a result, some MUs of the non-targeted fingers were also recruited. These MUs would be considered as interferences to the target finger force predictions because the separation

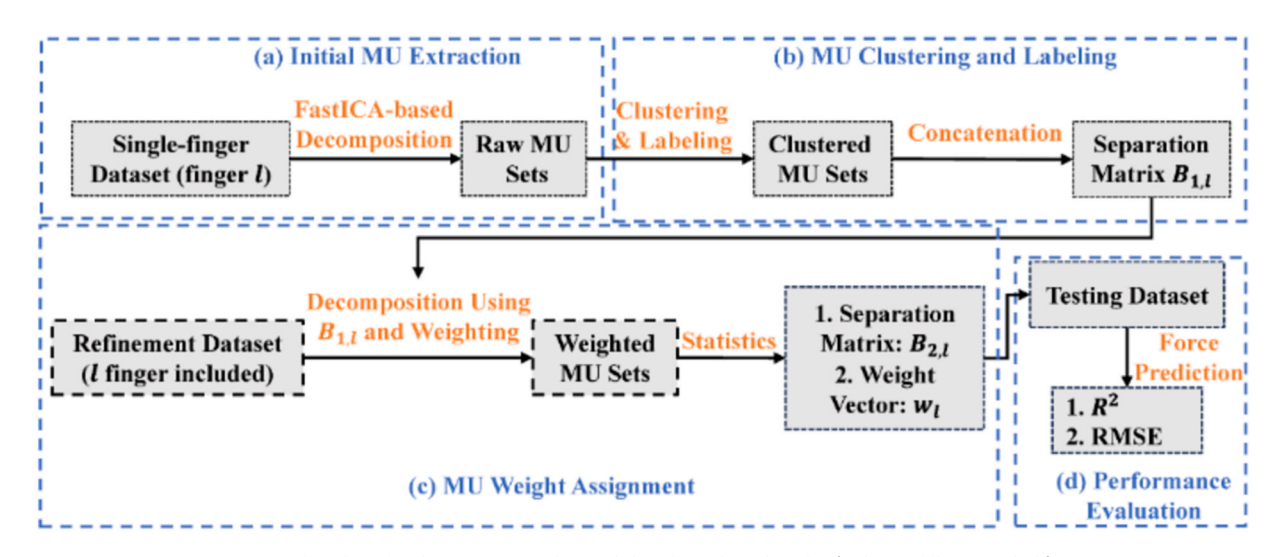


Fig. 4. Flowchart for the unsupervised neural decoding algorithm. $l \in \{index, middle, ring - little\}$.

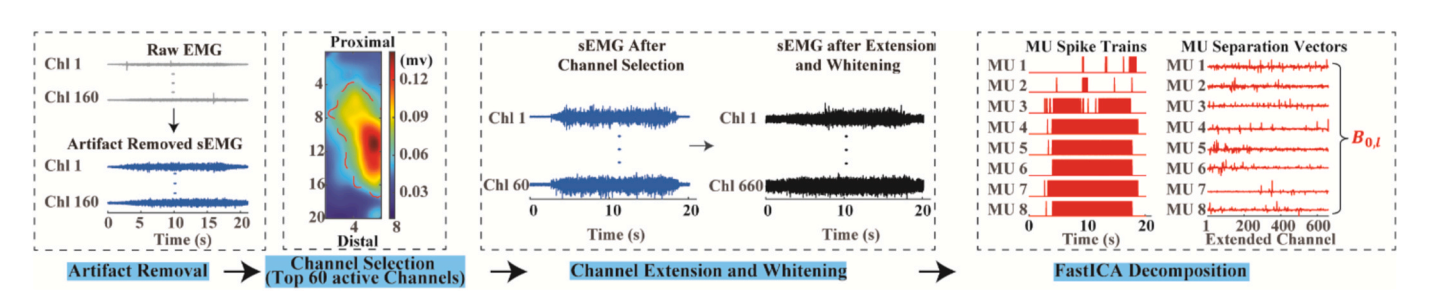


Fig. 5. Initial MU extraction procedure.

matrices of the single-finger tasks were applied directly to the sEMG signals of the multi-finger tasks. We, therefore, implemented the MU clustering and labeling processes to eliminate these MUs.

Fig. 6 shows the MU clustering and labeling procedure. For each single-finger trial, we first obtained a MU set and calculated corresponding time courses of firing rates using a sliding window. Based on the shape similarity of paired Kalman-filtered firing rate profiles measured by Dynamic Time Warping (DTW) [38], we employed the agglomerative hierarchical clustering [39] approach to obtain 3 clusters. The MU cluster having the largest mean population firing frequency was labeled as the target MU cluster. Then, the target MUs from the same finger were pooled together as the Clustered MU set for this finger. Correspondingly, their separation matrixes were concatenated to form $B_{1,l}$. Specifically, the MU labeling was conducted in the following procedures for each decomposed spike train set:

- (1) Obtain the time course of firing rates for each MU. To accurately estimate the time-varying firing rates of motor units (MUs), we initially applied a sliding window (window size: 0.5 s, sliding step size: 0.1 s) to convert spike occurrences (Fig. 7 (a)) into a firing rate time course (Fig. 7 (b)). Given the inherent variability in spike timing and the finite window size, this estimation process can introduce noise, manifested as sporadic, large-amplitude fluctuations in the estimated firing rates, as shown in Fig. 7 (c). To address these issues, we employed a Kalman filter smoothing process, tailored to our specific needs and data characteristics [40]. In our context, it was used to refine our firing rate estimates by iteratively predicting and correcting the state (i.e., the true firing rates) based on both the system's dynamics and the current noisy observations (i.e., the initially estimated firing rates). As suggested by the previous study [40], the implementation of the Kalman filter in our analysis was characterized by four key parameters: the observation covariance (0.5), system covariance (0.1), observation matrix (1), and system matrix (1). If not specified, the same Kalman filter settings were applied in the subsequent analyses.
- (2) Calculate the distance between two time courses of firing rates using DTW. One key factor affecting the performance of clustering is the way that quantifies the similarity between two datasets. Given the characteristics of MU recruitment and the impact of muscle fatigue, certain MUs may not synchronize with the variations in force, resulting in temporal shifts of the plateau phase. To address this issue, we adopted the DTW technique to measure the similarity of paired time courses of firing rates as the inter-object distance. DTW is a well-known approach to measure the similarity of time series sequences. Suppose two time series sequences, $\mathbf{u} = \{u_1, u_2, \dots, u_i, \dots, u_p\}$ and $\mathbf{v} = \{v_1, v_2, \dots, v_i, \dots, v_q\}$, where p and q denote the number of samples in u and v, respectively. DTW aims to minimize the difference between the two time series by the following alignment procedure: A distance matrix $D \in \mathbb{R}^{p \times q}$ is built, where the value of (i,j) element in D is the Euclidean distance between u_i and v_j . Then, DTW solves a

- minimum-distance path starting from D(0,0) to D(p,q) with two constraints: 1) neighboring points should be spatially adjacent, and 2) the warping path should move monotonically over time.
- (3) Cluster MUs by generating an agglomerative hierarchical cluster tree. The agglomerative hierarchical clustering [39] was a bottom-up clustering approach where each object (time courses of firing rate) was initially considered as a separate cluster. Then, two clusters with the shortest distance among all inter-cluster distances were merged as a new cluster until a tree of clusters was formed. We adopted the group average linkage as the strategy of measuring the inter-cluster to minimize the impact of potential outlier values. Based on the number of fingers involved in this study, the final number of clusters was set to 3. Compared with three prevailing unsupervised clustering techniques (KMeans++, KMedoids and AutoEncoder), we can achieve the best force prediction performance using the agglomerative hierarchical clustering. Refer to Section E in the Supplementary Material for details.
- (4) Determine the cluster for the target finger. After the clustering procedure, we calculated the mean population firing frequency of each cluster. As subjects were required to follow the force target trajectory using the target finger (with efforts to minimize the coactivation of other fingers) in the single-finger tasks, the MU cluster with the largest mean population firing frequency was considered to have a close association with the target finger and thus were selected for subsequent analyses.

The same procedures were performed for each single-finger trial. MUs from clusters related to the same finger were pooled together. Accordingly, three separation matrixes were obtained for the index, middle, and ring-little fingers, i.e., $B_{1,I}$, $B_{1,M}$ and $B_{1,RL}$, respectively. This was the preliminary categorization or labeling of MUs into different fingers. There is a high possibility that duplicated MUs exist in the clustered MU pool, those MUs would be removed in the subsequent analyses.

A representative example of the clustering effect is shown in Fig. 8. MUs in Fig. 8(c) and (d) and 8(e) were groups clustered from Fig. 8(b). Based on the time course of firing rates, it was clear that MUs in Fig. 8(c) and (e) and were not associated with the forces of the target finger. Correspondingly, those MUs were removed from subsequent analyses.

2.2.3. MU weight assignment

Because the FastICA decomposition is time-consuming and not feasible for real-time neural decoding, we directly applied the separation matrixes $B_{1,l}$ (i.e., $B_{1,l}$, $B_{1,M}$ or $B_{1,RL}$) obtained from the single finger tasks to decompose the refinement dataset of the multi-finger tasks, as shown in Fig. 9. This approach has been used for real-time decoding to obtain the firing events of specified MUs [40]. Suppose there were m multi-finger trials involving l finger in the refinement dataset, and a total of n MUs were decomposed using $B_{1,l}$. We used the same sliding window as in the clustering procedure to obtain the time courses of firing rates. Then, the Kalman filter was applied to smooth the filtered firing rate profiles. Because some MUs may be activated for the movement of more

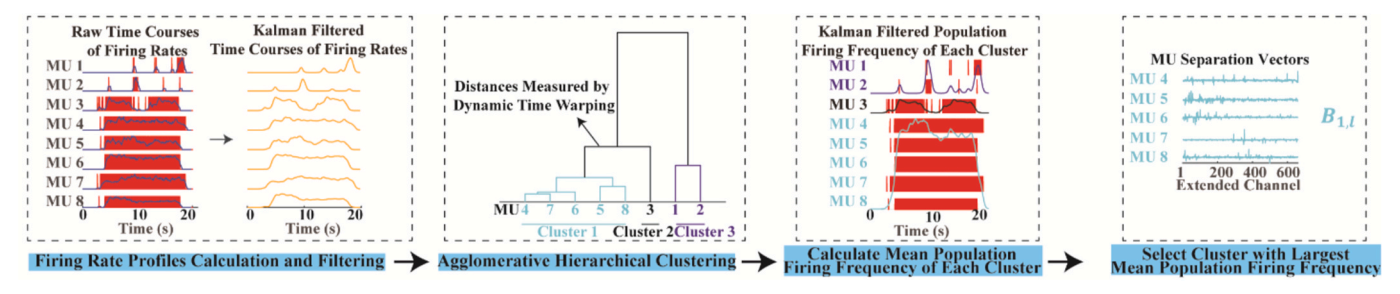


Fig. 6. MU clustering and labeling procedure. $l \in \{index, middle, ring - little\}$.

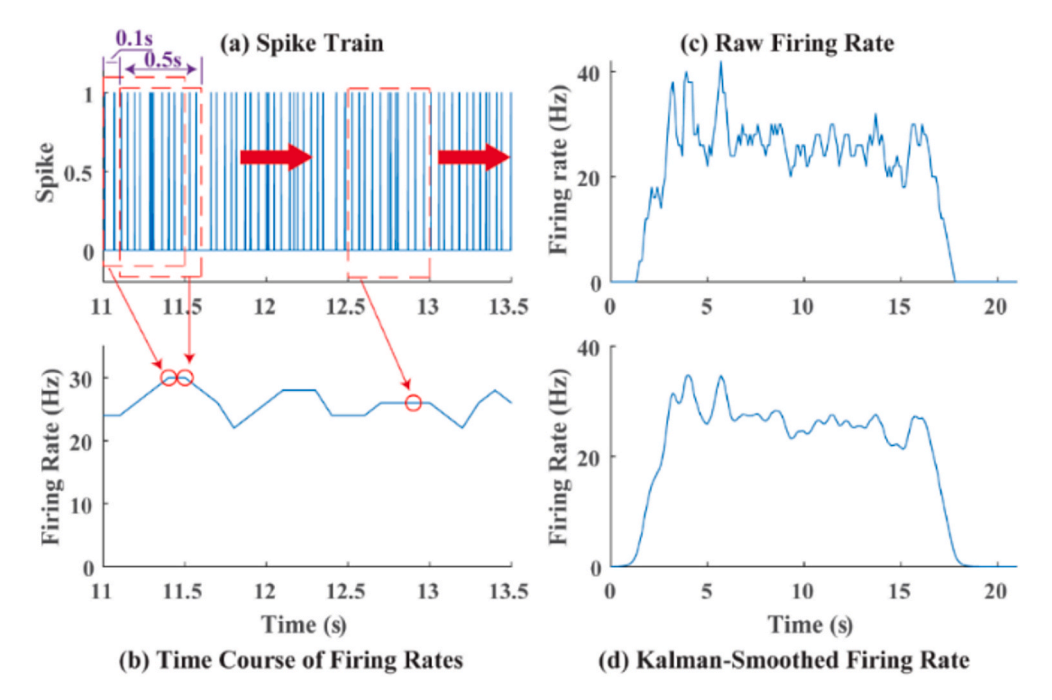


Fig. 7. A representative example of transforming the MU spike train (a) into a time course of firing rates (b) and Kalman filtering performance. (a) Spike train. (b) Time course of firing rates. (c) Raw time course of firing rate. (d) Kalman-smoothed firing rate. (b) Is the detailed representative of (c) from 11s to 13.5s.

than one finger, we assigned weights to MUs based on their contributions over trials using an unsupervised approach. For each firing rate profile, if the mean firing rate during the plateaus of the l finger was greater than the mean firing rate during the plateaus of other active fingers, we designated this MU to be dominated in the l-finger plateau period. The percentage of this MU retained across the m trials was used as the weight for this MU. To improve the effectiveness of decomposing MUs, we removed the MUs whose weights were 0. Then, we pooled the rest of the MUs together, obtaining the separation matrix $B_{2,l}$ and corresponding weight vector. The detailed procedures to assign weights are as follows:

- (1) Calculate the source signals $s_{i,l}$ ($i=1,2,\cdots,n_{1,l}$) by applying the separation vectors of $\boldsymbol{B}_{1,l}$ to multi-finger refinement dataset, where $n_{1,l}$ is the number of separation vectors in $\boldsymbol{B}_{1,l}$. Obtain firing event trains $t_{i,l}$ from $s_{i,l}$, remove the low-quality firing event trains (SIL<0.5), and obtain the time courses of firing rate ($f_{i,l}$) for each retained MU, where 1 < i < the number of retained MUs.
- (2) Select MUs closely related to the target finger. The rationale for this selection is that if the current MU is closely related to the target finger, the corresponding mean firing rate during the plateaus of the target finger should be higher than that during the plateaus of other untargeted fingers. Take one trial of the two-finger movements as an example, and suppose the index is the first finger shown in Fig. 3(b), for each MU obtained from $B_{1,l}$, we obtained the corresponding time courses of the firing rate $f_{i,l}$. If the mean firing rate of $f_{i,l}$ during the plateau period (i.e., 2s–4s) of the index finger force was larger than the mean firing rate of $f_{i,l}$ during the plateau period (i.e., 8s–10s) of the force trajectories of the second finger, the MU was retained for the next step.
- (3) Calculate the weight for each MU. Due to variations over different multi-finger trials, the retained MUs may vary with trials. To get a generalized MU set and emphasize the contribution of MUs closely related to the target finger, we calculated the weight for each MU as how often this MU was retained in the MU sets, i.e., $\frac{\text{the number of times this MU was retained}}{\text{the number of trials for weighting}}. Accordingly, we updated the separation matrix <math>\boldsymbol{B}_{1,l}$ to $\boldsymbol{B}_{2,l}$ by excluding the separation vectors

not meeting the requirement of step 2 across all included refinement trials. The related weight vector $w_{2,l}$ was associated to the separation vectors in $B_{2,l}$ for the index finger.

To intuitively illustrate this part, we presented the population discharge frequency for the movement of the middle finger (Fig. 10). The MUs were ranked based on their assigned weights. The height of each spike train was multiplied by its weight. As shown in Fig. 10, MUs with high weights were more specific to the target finger than those with low weights. By emphasizing the MUs with high contributions and reducing the effect of cross-finger MUs, the force prediction accuracy can be improved.

2.2.4. Force prediction

Fig. 11 Shows the force prediction procedure for a testing trial. We first decomposed the testing trial using the three separation matrixes $(B_{2.index}, B_{2.middle}, B_{2.ring-little})$ for the index, middle, and ring-little finger, respectively. Then, we obtained the population firing frequency of each finger by multiplying the spike trains with their corresponding weights and summed the weighted spike trains. Same as the previous study [28], a linear model was built to map the neural drive signals to the force of the target finger of each finger. Note that the measured force was only used for the performance evaluation without being utilized in any of the MU extraction, clustering, labeling, or weighting procedures. Because the neural drive signals are generally linear to the finger force, users can easily scale the prediction models by their subjective perception of finger force levels. The practical use is not affected in scenarios where the actual finger force cannot be measured.

For each multi-finger trial in the testing dataset, we constructed three separate models to estimate the forces of the three fingers. Using the l finger as an example, we first obtained the source signals of MUs using $B_{2,l}$, and excluded low-quality firing event trains (SIL<0.6). Then, we removed duplicated source signals. Some source signals may represent the activity of the same MU. After regulating the time delay within ± 2.5 ms, any pair of two firing event trains was considered as a duplicate if 80% of synchronized spike events were detected. The duplicated source signal with a lower SIL was removed from subsequent analyses. Accordingly, the time courses of firing rates and the weight vector

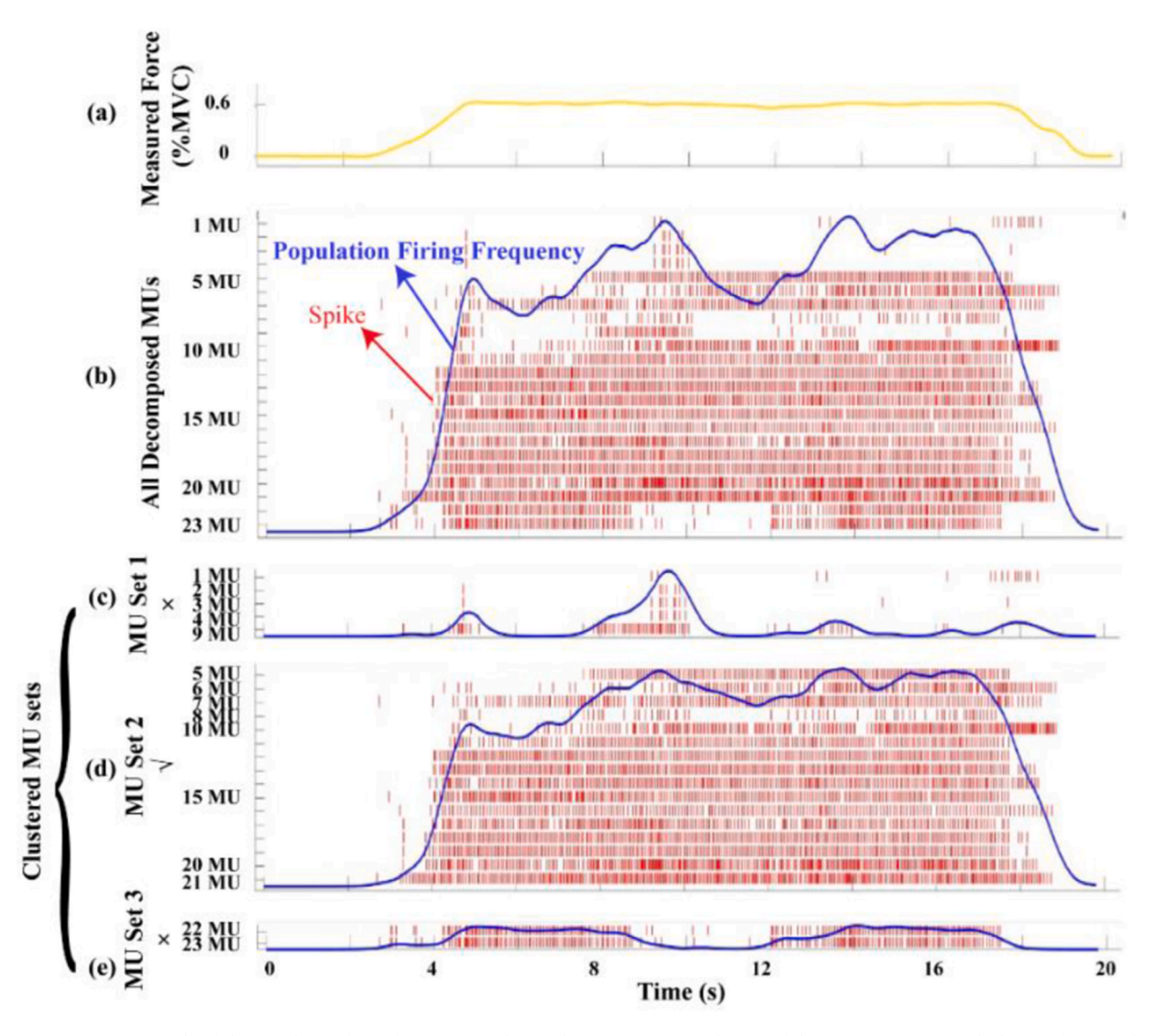


Fig. 8. A representative example of the population firing frequency of clustered MUs. (a) Measured force of the representative ring-little (RL) finger task. We obtained the raw MUs (b) by decomposing the sEMG signals from the RL finger task. The raw MUs were then clustered into three groups, shown in (c), (d), and (e), respectively. The MU set in (d) having the largest population firing frequency was selected as the MU set closely related to the target finger.

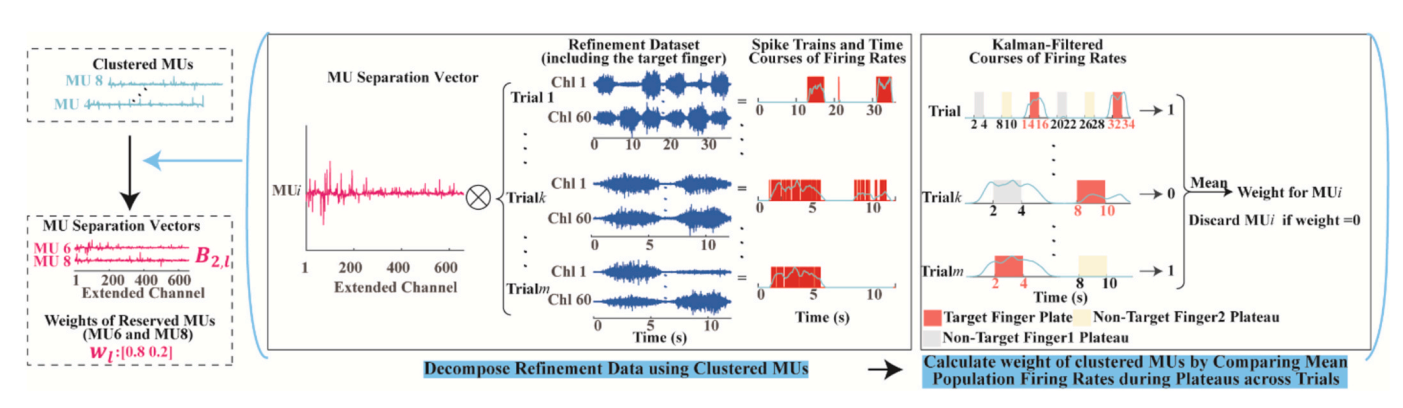


Fig. 9. MU weight assignment procedure for l finger. $l \in \{index, middle, ring - little\}$.

updated as $F_l = [f_{1,l}, f_{2,l}, \cdots, f_{i,l}, \cdots f_{n_l,l}]$ and $w_l = [w_{1,l}, w_{2,l}, \cdots, w_{i,l}, \cdots w_{n_l,l}]$, where $f_{i,l}$ and $w_{i,l}$ denote the time course of firing rate and the weight for the i th MU, n_l denotes the number of retained high-quality MUs after this step. The neural drive time series signals $D_l = \sum_i f_{i,l} \bullet w_{i,l}$. After smoothing D_l with the Kalman filter, we used the neural drive signals to

predict the force using a linear regression model.

$$Force_{l}^{Tst} = a_{l} \mathbf{D}_{l} + b_{l} \tag{1}$$

where $Force_l$ indicates the estimated force of the index finger, a_l and b_l represent the slope coefficient and intercept of the model, respectively.

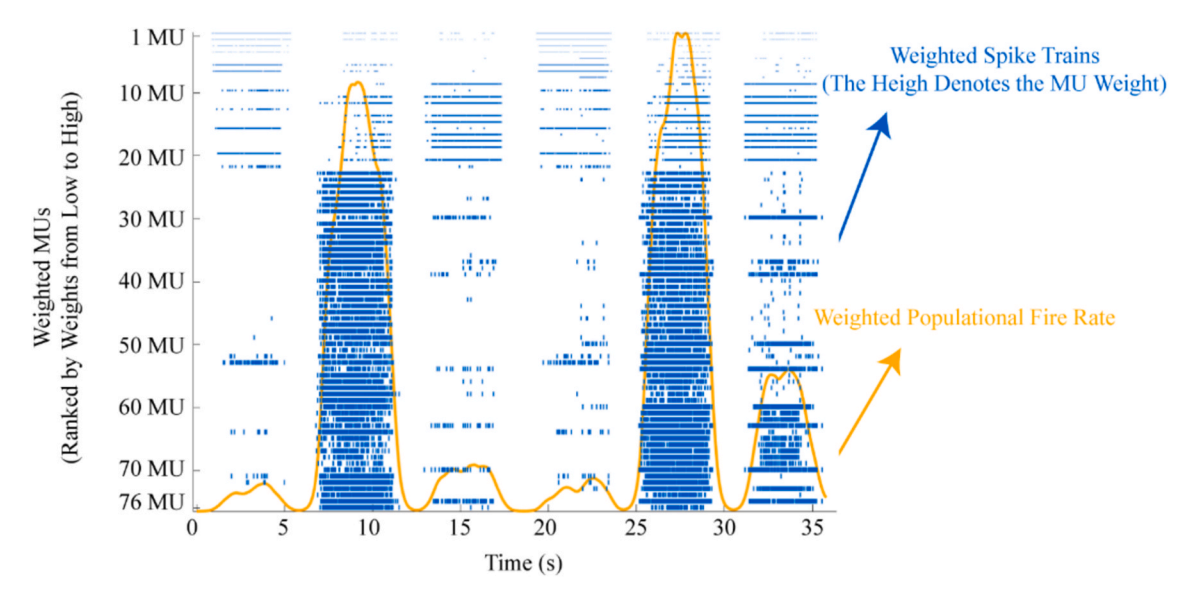


Fig. 10. Representative population discharge frequency using weighted MUs for the middle finger. The yellow trajectory represents the weighted neural drive. The MUs were ranked based on their weights, and the heights of the spike trains denote the relative weight values.

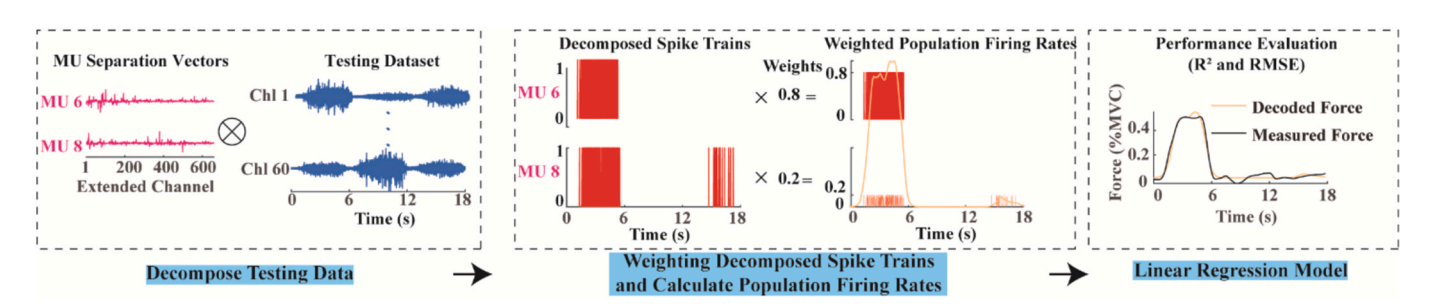


Fig. 11. Force prediction procedure for a testing trial.

The performance of force prediction was quantified using the coefficient of determination (R^2) and the root mean square error (RMSE) value between the measured force and the estimated force. We selected the R^2 and RMSE as two complementary metrics due to their relevance and widespread acceptance in the field of neural decoding and motor control prediction. The R^2 metric provides insight into the proportion of variance in the dependent variable (multi-finger forces) that is predictable from the independent variables. The equation for R^2 can be expressed as:

$$R^{2} = 1 - \frac{\sum_{i=1}^{n} (y_{i} - \widehat{y}_{i})^{2}}{\sum_{i=1}^{n} (y_{i} - \overline{y})^{2}}$$
 (2)

where y_i denotes the actual value of the i th observation, \hat{y}_i denotes the predicted value for the i th observation, $\bar{y} = \frac{1}{n} \sum_{i=1}^{n} y_i$ denotes the mean of the actual values and n denotes the number of observations.

RMSE, on the other hand, provides a clear measure of the magnitude of prediction errors, offering an intuitive understanding of the average error magnitude in the same units as the predicted variable. Mathematically, RMSE is defined as follows:

$$RMSE = \sqrt{\frac{1}{n} \sum_{i=1}^{n} (y_i - \hat{y}_i)^2}$$
 (3)

where y_i denotes the actual value of the i th observation, \hat{y}_i denotes the predicted value for the i th observation and denotes the number of observations.

2.3. Alternative methods for comparison

2.3.1. Unsupervised neural decoding using phase amplitude

Considering subtle changes of a time-dependent variable can be revealed in the phase plane (the variable against one time derivative of the variable), we provided an alternative perspective for force prediction using the phase amplitude instead of the firing rate information. Given the time course of firing rate f, the corresponding time course of phase amplitude can be obtained via $\sqrt[2]{f^2 + \left(\Delta f_{/\Delta t}\right)^2}$. To explore the force prediction performance using the phase amplitude, all the firing rates used in Section 2.2 were replaced with the phase amplitudes for the MU clustering, labeling, weight assignment, and force prediction calculations.

2.3.2. Supervised neural decoding

A recent study [28] developed a supervised neural decoding approach for force prediction, in which the measured forces were used for the MU pool refinement. The supervised neural decoding approach first extracted MUs from single-finger tasks. MUs related to the same target finger were pooled together. The key step was to calculate the average R^2 between each MU and three finger forces across trials in the refinement dataset. If MUs had the highest mean R^2 with the target finger force, the MUs were retained for the force prediction. Refer to Section C in the Supplementary Material for detailed procedures of force prediction using the supervised approach.

2.3.3. sEMG amplitude-based force prediction

The force prediction was also conducted using a conventional sEMG amplitude method (a preferred feature for force prediction [41]) as a comparison. The interference from channel-crosstalk on sEMG amplitude could potentially introduce a bias in force prediction. The finger muscle compartments also have different spatial distributions. Therefore, we performed a channel-refinement procedure developed in a previous study [28] to minimize the channel interference. To be specific, we first selected top 60 channels with maximum average sEMG amplitude (RMS value) for three fingers based on single-finger trials (motion artifacts of sEMG signals have been removed prior to the RMS calculation). Then, we calculated the average \mathbb{R}^2 between the sEMG amplitude of each channel and three measured forces across trials in the refinement dataset. We retained the channels having a higher R^2 with the target finger than that with other fingers for the final force prediction. Refer to Section D in the Supplementary Material for detailed procedures of sEMG amplitude-based force prediction.

2.4. Statistical analysis

We performed statistical analyses to evaluate the force prediction performance. First, if the compared groups satisfied the Gaussian distribution assumption (indicated by the Shapiro-Wilk test) and met the assumption of sphericity (indicated by the Mauchly's test, for comparisons involving at least three groups), we adopted the parametric analysis (paired t-test for two group comparison, and Repeated Measures Analysis of Variance (ANOVA) for multi-group comparisons). Otherwise, the non-parametric analysis approach (Wilcoxon signed-rank test or Friedman test) was applied for the statistical analysis. When applicable after ANOVA or Friedman tests, Holm-Bonferroni correction was employed to avoid multiple-comparison errors. The significance level was set to 0.05 and only the corrected p values were reported in this study.

3. Results

3.1. Comparison of the unsupervised and supervised neural decoding approaches

First, we were able to predict multi-finger force with a computational delay of 79 ± 31.5 ms using an AMD Ryzen 7 6800H @ 3.2 GHz with 64 GB of memory environment. This delay is sufficient to meet the daily needs of real-time human-robot interactions, for which an acceptable loop delay ranges between 100 ms and 150 ms [42,43]. Force prediction performances using unsupervised, supervised, and sEMG amplitude (sEMG-Amp) approaches are shown in Fig. 12. The unsupervised approach was implemented using the firing rate information based on the weighted MU. Fig. 12(a) shows a representative force prediction using the three approaches. The unsupervised or supervised neural-decoding approaches can accurately predict the measured force. In contrast, the force predictions using the sEMG-Amp deviated substantially from the measured forces, resulting in large estimation errors. As shown in Fig. 12(b), the overall average R^2 values using unsupervised, supervised, and sEMG-Amp methods were 0.77 \pm 0.036, 0.71 \pm 0.11, and 0.61 \pm 0.09, respectively. The overall average RMSE values (Fig. 12(c)) were 5.16 \pm 0.58 %MVC (unsupervised), 5.88 \pm 1.34 % MVC (supervised), and 7.56 \pm 1.60 %MVC (sEMG-Amp). One-way repeated-measures ANOVA demonstrated significant differences for both R^2 (F (2,14) = 12.29, p < 0.001) and RMSE (F (2,14) = 10.61, p = 0.0016). Further post-hoc analyses revealed that the R^2 using either unsupervised or supervised approaches was significantly larger than that using the sEMG-Amp approach (both p < 0.05). Besides, the R^2 using the unsupervised method was significantly smaller than that using the sEMG-Amp approach (p = 0.0051).

The force prediction performances for each finger are shown in Fig. 12(d) and (e) and. The comparisons of R^2 were significantly different for the index finger (F (2,14) = 5.46, p = 0.018) and the ringlittle finger (F (2,14) = 22.05, p < 0.001). Further post-hoc analyses revealed that R^2 obtained using either the unsupervised or supervised method was significantly better than that using the sEMG-Amp method for the ring-little finger (both p < 0.01). Besides, the R^2 value obtained using unsupervised approach was significantly larger than that using sEMG-Amp approach for the index finger (p = 0.01). For the comparison

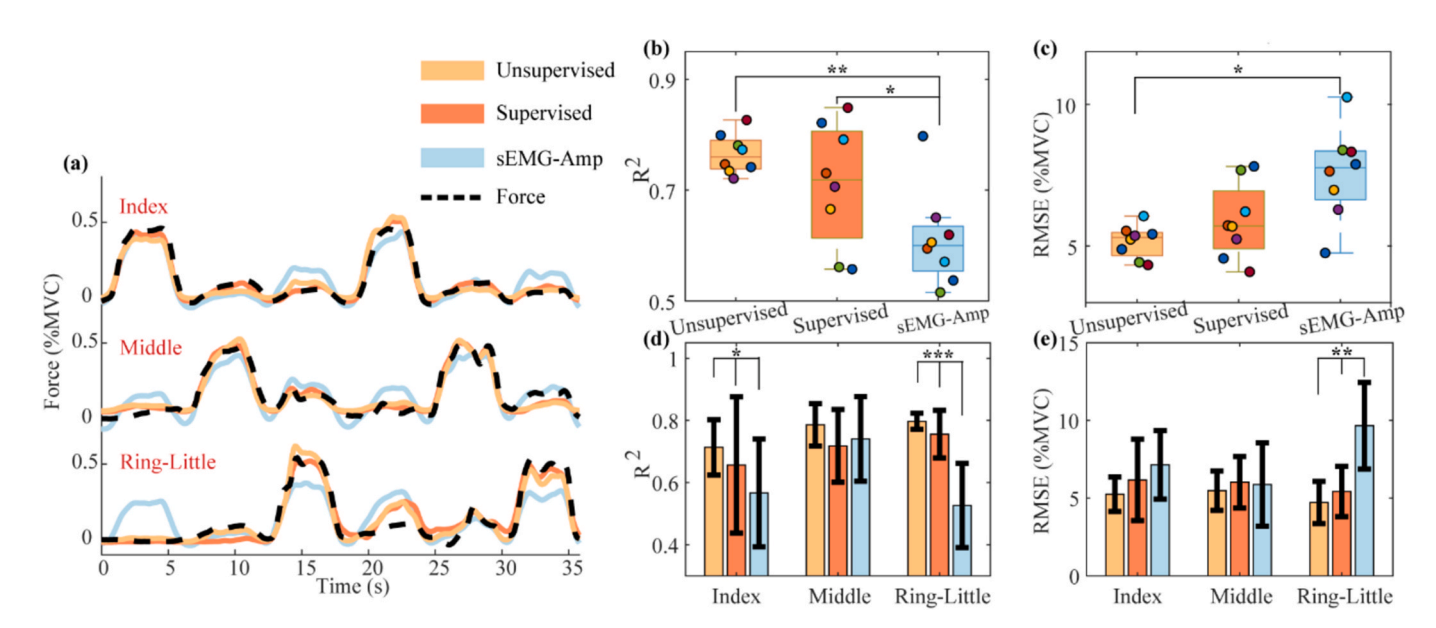


Fig. 12. Comparison of the unsupervised and supervised neural decoding approaches. (a) A representative force prediction using the unsupervised neural decoding, supervised neural decoding and sEMG amplitude-based approach. (b) Overall Interquartile range of R^2 value. (c) Overall Interquartile range of RMSE value. In both (b) and (c), each colored dot represents the average R^2 or RMSE value for a subject. (d) Average R^2 value for each finger. (e) Average RMSE value for each finger. The length of error bars indicates the standard error. * denotes 0.01 , ** denotes <math>0.001 , *** denotes <math>p < 0.001.

of RMSE, the Friedman test demonstrated a significant difference for the ring-little finger (χ^2 (2) = 13, p = 0.0015). The pair-wise comparison showed that the RMSE value obtained using either the unsupervised or the supervised approach was significantly smaller than that using the sEMG-Amp approach for the ring-little finger (both p < 0.05). Besides, the RMSE value using the unsupervised approach was significantly lower than that using the supervised approach for the ring-little finger (p = 0.027).

3.2. Evaluating the effect of MU clustering and weighting procedures

We compared the performance of three different unsupervised neural drive-based force prediction methods (Fig. 13): The first directly used MUs (termed raw MU) decomposed from single-finger tasks without any clustering and weighting, the second clustered and labeled MUs (termed clustered MU) related to the target fingers, and the third assigned a weight to each MU (termed weighted MU). We initially averaged the performance index (R2 value and RMSE value) across all trials in the testing dataset, and then across all fingers. The overall average R^2 values (Fig. 13(a)) were 0.77 \pm 0.036 (weighted MU), 0.69 \pm 0.063 (clustered MU), and 0.68 \pm 0.063 (raw MU). The overall average RMSE values (Fig. 13(b)) were 5.16 \pm 0.58 %MVC (weighted MU), 6.37 \pm 0.91 % MVC (clustered MU), and 6.56 \pm 0.90 %MVC (raw MU). One-way repeated-measures ANOVA demonstrated that the force prediction performances using different methods were significantly different in both R^2 (F (2,14) = 19.09, p <0.001) and RMSE (F (2,14) = 19.79, p <0.001). Further post-hoc test revealed that the R^2 using the weighted MU was significantly larger than those using the clustered MU and the raw MU (both p < 0.01), and the R^2 value using the clustered MU was significantly higher than that using the raw MU (p = 0.013). Similarly, the RMSE using the weighted MU was significantly smaller than those using the clustered MU and the raw MU (both p < 0.01). The RMSE using the clustered MU was also significantly lower than that using the raw MU (p = 0.006).

We also compared the force prediction performance for individual fingers, as shown in Fig. 13(c) and (d) and. For the comparison of \mathbb{R}^2 , since the results using the cluster MU and raw MU did not follow Gaussian distribution, we used the Friedman to test the overall

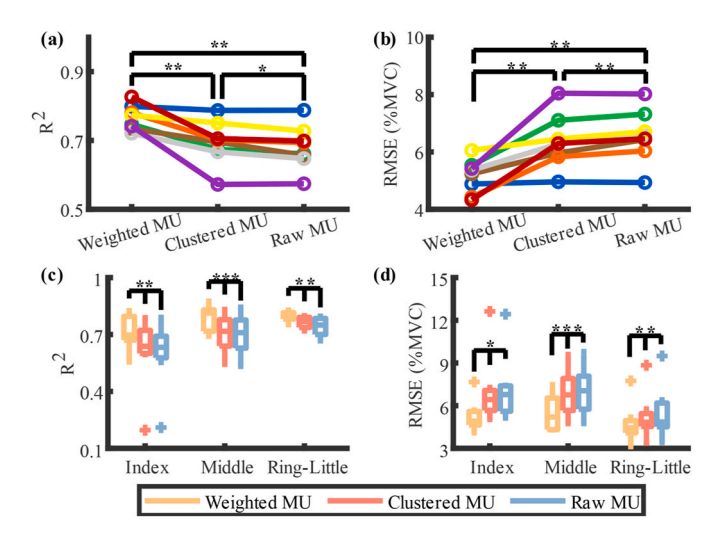


Fig. 13. Force prediction performance using three different MU-based neural decoding methods. (a) Average R^2 value for each subject. (b) Average RMSE value for each subject. Each colored circle represents the mean R^2 in (a) and RMSE value in (b) of individual subjects. (c) Interquartile range of R^2 value for each finger. (d) Interquartile range of RMSE value for each finger. The error bars in (a) and (b) denote the standard error. The "+" in (c) and (d) denote outliers. * denotes 0.01 , ** denotes <math>0.001 , *** denotes <math>p < 0.001.

difference, and conducted the pair-wise comparison using the Wilcoxon signed-rank test for the index finger. Statistical analysis revealed that significant differences were observed for each finger (i.e., index: χ^2 (2) = 9.75, p=0.0076, middle: F (2,14) = 12.8, p <0.001, ring-little: F (2,14) = 7.34, p=0.007). Further post-hoc analyses showed that the R^2 value obtained using the weighted MU was significantly larger than that using either the clustered MU or the raw MU (both p <0.05) for each finger. Similarly, significant differences in the RMSE values were observed for each finger (i.e., index: χ^2 (2) = 7, p=0.03, middle: F (2,14) = 13.48, p <0.001, ring-little: χ^2 (2) = 10.75, p=0.0046). The post-hoc analyses showed that the RMSE value using the weighted MU was significantly smaller than that using either the clustered MU or the raw MU (both p <0.05) for each finger. The RMSE using the clustered MU was also significantly lower than that using the raw MU for the middle finger (p=0.011).

3.3. Comparison of performance using firing rate and phase amplitude

We explored the force prediction performance using the phase amplitude of the firing rate based on the weighted MU, as shown in Fig. 14. The average R^2 values obtained using the firing rate and phase amplitude were 0.77 ± 0.036 and 0.75 ± 0.022 , respectively (Fig. 14 (a)). The paired t-test showed no significant difference for the R^2 using the firing rate and the phase amplitude (t(7) = 1.18, p = 0.28). The average RMSE using the firing rate and phase amplitude were 5.16 ± 0.58 %MVC and 5.58 ± 0.76 %MVC, respectively (Fig. 14(b)). The paired t-test showed no significant difference for the RMSE using the firing rate and the phase amplitude (t(7) = -1.44, t = 0.19).

To investigate finger-specific difference, the two measurements were averaged across trials in the testing dataset (Fig. 14(c) and (d)) for individual fingers. For the R^2 evaluation, the obtained results for the middle finger using phase amplitude did not follow Gaussian distribution (p=0.037). Accordingly, the Wilcoxon signed-rank test showed no significant difference between the firing rate and phase amplitude for the middle finger (p=0.38). The paired t-test revealed that the firing rate was significantly better than the phase amplitude for the ring-little finger (t(7)=3.57, p=0.0045), but no significant difference was found between the two approaches for the index finger (t(7)=-0.68, p=0.52). For the RMSE evaluation, the obtained results using the firing rate for the index finger (p=0.033) did

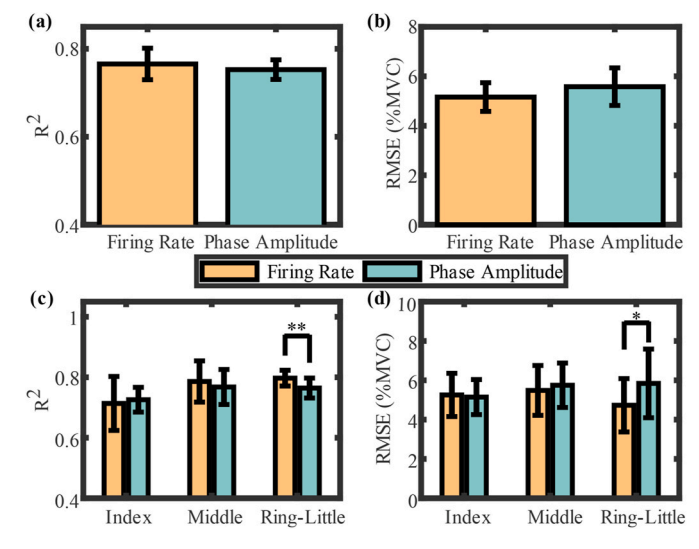


Fig. 14. Force prediction performances using the firing rate and the phase amplitude. (a) Overall average R^2 value. (b) Overall average RMSE value; (c) Average R^2 value for each finger; (d) Average RMSE value for each finger. The length of the error bars indicates the standard error. * denotes 0.01 , ** denotes <math>0.001 .

not follow Gaussian distribution. Statistical analysis indicated that the firing rate was significantly better than phase amplitude for the ring-little finger (Wilcoxon signed-rank test: p=0.012), and no significant difference between the two approaches for the index finger (Wilcoxon signed-rank test: p=0.46) and the middle finger (paired test: t(7)=-0.89, p=0.41).

4. Discussion

In this study, we aimed to decode the sEMG signals for concurrent and continuous multi-finger force prediction in an unsupervised manner. We decomposed HD-sEMG signals using the FastICA algorithm to extract raw MUs from single-finger tasks. The decomposed MUs were then clustered and labeled for individual fingers. The clustered MUs were assigned weights based on the consistency of being retained during the plateau period of the refinement dataset. The population firing frequency of weighted MUs was utilized for the extension force prediction of each finger. The results revealed that the force prediction accuracy improved significantly using MU clustering and weighting procedures. The outcomes demonstrated the feasibility of unsupervised neural decoding using MU firing activities.

The improvement of force prediction performance using the unsupervised neural decoding may arise from several factors. First, it is common to recruit MUs in muscle compartments associated with untargeted fingers [29–31] due to the enslavement effect across fingers. The MU clustering procedure can remove some of these MUs prior to neural drive calculation. Second, the force prediction was further improved using the weighted MUs. The weighting procedure can assign large weights to MUs specially aligned with the target finger. Finally, the clustering and weighting procedures may also remove or attenuate the effect of inaccurate MU spikes. Although the separate vectors were filtered initially. Earlier work has shown that the SIL index only has a moderate correlation with the spike detection accuracy [44,45]. The clustering procedure could remove these MUs from the pool, and the weighting procedures can assign smaller weights to these MUs potentially due to inconsistent MU presence across activation trials.

Our study revealed that prediction accuracy (R^2) using the neural decoding approaches was significantly better than that using the sEMG-Amp method, which was attributed to multiple factors. The finger muscle compartments are spatially close to each other and are even partially overlapped from the viewpoint of skin surface, some sEMG channels are corrupted due to crosstalk of multiple muscle compartments, and this can lead to inaccurate force predictions. Even though the channel refinement in the sEMG-Amp approach reduced the influence of crosstalk, remaining channels may still be impacted by this interference. As a comparison, the neural decoding methods decomposed MUs from single-finger tasks. This critical step in classifying or clustering MUs specific to each finger ensured that neural drive signals can be concurrently and independently estimated for each finger even when muscle compartments were located in close proximity to each other. Compared with the supervised approach, the unsupervised method can achieve a competitive result. The variability in performance between subjects using our unsupervised prediction model was found to be lower than that observed with the supervised approach, demonstrating its enhanced consistency and robustness across different individuals. As a crucial step, the supervised neural decoding distinguished MUs specific to the target finger by comparing the R^2 between the time course of one MU with the force of each finger. In contrast, we introduced the clustering step to exclude MUs not related to the target finger. Then, to emphasize the MUs with a high consistency of MU inclusion in the target finger activation trials and minimize the impact of cross-finger MUs, we performed the weighting step by assigning different weights to clustered MUs. Our results show that both the clustering and weighting procedures can contribute to accurate force predictions.

As an alternative to MU firing rate, we also used the phase amplitude

to perform MU clustering, weighting, and finger force predictions. The phase amplitude in the phase plane incorporates the amplitude of the firing rate as well as the change of firing rate. However, it was unexpected that the phase amplitude of the firing rate did not outperform the direct firing rate calculation for finger force predictions. The phase amplitude and firing rate time series signals are highly correlated, which can partly explain their similar performance in force predictions. In our current study, we did not incorporate the phase angle information at any stage of the algorithm procedures. It is worth exploring how dynamic information of the MU firing activities can be further leveraged to improve the decoding accuracy.

Although we have achieved a promising result using the unsupervised approach, this study has limitations. First, only isometric finger force was included. In future studies, we can validate the developed unsupervised method for finger force prediction during dynamic finger movement tasks. Second, one advantage of the unsupervised approach was that it was suitable for individuals with hand disabilities. However, all the participants in the current study were able-bodied individuals. For transradial amputees, the available stump areas may not be suited for the electrode array placement. Besides, the neuromuscular system might undergo changes after amputation. The way muscles receive and interpret signals in the brain can be different from able-bodied people. In future work, we can employ subjects with hand disabilities to further test the developed unsupervised approach. Third, our study focused on the four fingers, excluding the thumb due to its unique anatomy and movement capabilities, which our sEMG data from forearm muscles could not accurately capture, thus limiting our analysis. In future work, we can extend our data collection to include sEMG signals from the thumb's intrinsic muscles, which will enable us to validate our neural decoding algorithms on the thumb force prediction. Fourth, the separation matrix of the single-finger tasks was directly applied to the multifinger tasks. However, it is likely that new MUs were active during the multi-finger tasks, but our current procedure could not identify these new MUs. Further investigations that can capture these newly recruited MUs using an adaptive decomposition algorithm [46] may help improve the decoder accuracy. Lastly, we will conduct further validation using suitable single-finger and multi-finger sEMG datasets when they become available.

5. Conclusion

In summary, we developed an unsupervised neural decoding approach to predict multi-finger forces concurrently and continuously in real-time, in which MUs extracted from the single-finger tasks were clustered and weighted for individual fingers in an unsupervised manner. Our new MU clustering and refining approach has been proven to be effective for accurate finger force prediction. Compared with the supervised neural decoding approach, the proposed method can achieve a consistently high accuracy across participants. Our findings offer a foundation for expanding the scope of the neural-machine interface. With further improvement, our approach has the potential to help improve or restore motor functions in individuals with hand disabilities.

CRediT authorship contribution statement

Long Meng: Conceptualization, Data curation, Formal analysis, Investigation, Methodology, Software, Validation, Visualization, Writing – original draft, Writing – review & editing. **Xiaogang Hu:** Conceptualization, Funding acquisition, Investigation, Project administration, Resources, Supervision, Writing – review & editing.

Declaration of competing interest

None Declared.

Acknowledgments

This study was supported in part by the National Science Foundation (CBET-2246162, IIS-2330862, IIS-2319139) and the Department of Defense (W81XWH2110185).

Appendix A. Supplementary data

Supplementary data to this article can be found online at $\frac{\text{https:}}{\text{doi.}}$ org/10.1016/j.compbiomed.2024.108384.

References

- B.N. Perry, C.W. Moran, R.S. Armiger, P.F. Pasquina, J.W. Vandersea, J.W. Tsao, Initial clinical evaluation of the modular prosthetic limb, Front. Neurol. 9 (2018) 153
- [2] Z. Wang, H. Wan, L. Meng, Z. Zeng, M. Akay, C. Chen, W. Chen, Optimization of inter-subject sEMG-based hand gesture recognition tasks using unsupervised domain adaptation techniques, Biomed. Signal Process Control 92 (2024) 106086.
- [3] Q. Wu, Y. Zhang, J. Liu, J. Sun, A. Cichocki, F. Gao, Regularized group sparse discriminant analysis for P300-based brain–computer interface, Int. J. Neural Syst. 29 (6) (2019) 06.
- [4] A. Ortiz-Rosario, I. Berrios-Torres, H. Adeli, J.A. Buford, Combined corticospinal and reticulospinal effects on upper limb muscles, Neurosci. Lett. 561 (2014) 30–34.
- [5] T. Lenzi, S.M.M. De Rossi, N. Vitiello, M.C. Carrozza, Intention-based EMG control for powered exoskeletons, IEEE (Inst. Electr. Electron. Eng.) Trans. Biomed. Eng. 59 (8) (2012) 8.
- [6] J.A. Barios, S. Ezquerro, A. Bertomeu-Motos, M. Nann, Fco J. Badesa, E. Fernandez, S.R. Soekadar, N. Garcia-Aracil, Synchronization of slow cortical rhythms during motor imagery-based brain-machine interface control, Int. J. Neural Syst. 29 (5) (2019) 05.
- [7] M.-C. Corsi, M. Chavez, D. Schwartz, L. Hugueville, A.N. Khambhati, D.S. Bassett, F. De Vico Fallani, Integrating EEG and MEG signals to improve motor imagery classification in brain-computer interface, Int. J. Neural Syst. 29 (1) (2019) 01.
- [8] V. Aggarwal, M. Mollazadeh, A.G. Davidson, M.H. Schieber, N.V. Thakor, State-based decoding of hand and finger kinematics using neuronal ensemble and LFP activity during dexterous reach-to-grasp movements, J. Neurophysiol. 109 (12) (2013) 3067–3081.
- [9] A. Ahmadi, A. Khorasani, V. Shalchyan, M.R. Daliri, State-based decoding of force signals from multi-channel local field potentials, IEEE Access 8 (2020) 159089–159099.
- [10] B. Farrokhi, A. Erfanian, A state-based probabilistic method for decoding hand position during movement from ECoG signals in non-human primate, J. Neural. Eng. 17 (2) (2020) 026042.
- [11] S.M. Hosseini, V. Shalchyan, State-based decoding of continuous hand movements using EEG signals, IEEE Access (2023).
- [12] X. Jiang, L. Meng, X. Liu, J. Fan, X. Ye, C. Dai, W. Chen, Optimizing the cross-day performance of electromyogram biometric decoder, IEEE Internet Things J. 10 (5) (2022) 4388–4402.
- [13] Y. Liu, Y. Ning, S. Li, P. Zhou, W.Z. Rymer, Y. Zhang, Three-dimensional innervation zone imaging from multi-channel surface EMG recordings, Int. J. Neural Syst. 25 (6) (2015) 06.
- [14] J. Fan, X. Jiang, X. Liu, L. Meng, F. Jia, C. Dai, Surface EMG feature disentanglement for robust pattern recognition, Expert Syst. Appl. 237 (2024) 121224
- [15] A. Fougner, Ø. Stavdahl, P.J. Kyberd, Y.G. Losier, P.A. Parker, Control of upper limb prostheses: terminology and proportional myoelectric control—a review, IEEE Trans. Neural Syst. Rehabil. Eng. 20 (5) (2012) 5.
- [16] D. Leonardis, M. Barsotti, C. Loconsole, M. Solazzi, M. Troncossi, C. Mazzotti, V. P. Castelli, C. Procopio, G. Lamola, C. Chisari, An EMG-controlled robotic hand exoskeleton for bilateral rehabilitation, IEEE Transactions on Haptics 8 (2) (2015)
- [17] A.A. Adewuyi, L.J. Hargrove, T.A. Kuiken, An analysis of intrinsic and extrinsic hand muscle EMG for improved pattern recognition control, IEEE Trans. Neural Syst. Rehabil. Eng. 24 (4) (2015) 4.
- [18] Z. Lu, X. Chen, X. Zhang, K.-Y. Tong, P. Zhou, Real-time control of an exoskeleton hand robot with myoelectric pattern recognition, Int. J. Neural Syst. 27 (5) (2017) 05.
- [19] L. Meng, Q. Chen, X. Jiang, X. Liu, J. Fan, C. Dai, W. Chen, Evaluation of decomposition parameters for high-density surface electromyogram using fast independent component analysis algorithm, Biomed. Signal Process Control 75 (2022) 103615.
- [20] L. Meng, X. Jiang, X. Liu, J. Fan, H. Ren, Y. Guo, H. Diao, Z. Wang, C. Chen, C. Dai, User-tailored hand gesture recognition system for wearable prosthesis and

- armband based on surface electromyogram, IEEE Trans. Instrum. Meas. 71 (2022)
- [21] Y. Guo, J. Liu, Y. Wu, X. Jiang, Y. Wang, L. Meng, X. Liu, F. Shu, C. Dai, W. Chen, sEMG-based inter-session hand gesture recognition via domain adaptation with locality preserving and maximum margin, Int. J. Neural Syst. 34 (3) (2024), 2450010–2450010.
- [22] J.G. Ngeo, T. Tamei, T. Shibata, Continuous and simultaneous estimation of finger kinematics using inputs from an EMG-to-muscle activation model, J. NeuroEng. Rehabil. 11 (1) (2014) 1.
- [23] J.N. Leijnse, N.H. Campbell-Kyureghyan, D. Spektor, P.M. Quesada, Assessment of individual finger muscle activity in the extensor digitorum communis by surface EMG, J. Neurophysiol. 100 (6) (2008) 6.
- [24] D. Farina, I. Vujaklija, M. Sartori, T. Kapelner, F. Negro, N. Jiang, K. Bergmeister, A. Andalib, J. Principe, O.C. Aszmann, Man/machine interface based on the discharge timings of spinal motor neurons after targeted muscle reinnervation, Nat. Biomed. Eng. 1 (2) (2017) 2.
- [25] R. Roy, Y. Zheng, D.G. Kamper, X. Hu, Concurrent and continuous prediction of finger kinetics and kinematics via motoneuron activities, IEEE (Inst. Electr. Electron. Eng.) Trans. Biomed. Eng. 70 (6) (2023) 1911–1920.
- [26] N. Rubin, Y. Zheng, H. Huang, X. Hu, Finger force estimation using motor unit discharges across forearm postures, IEEE (Inst. Electr. Electron. Eng.) Trans. Biomed. Eng. 69 (9) (2022) 2767–2775.
- [27] Y. Zheng, X. Hu, Concurrent estimation of finger flexion and extension forces using motoneuron discharge information, IEEE (Inst. Electr. Electron. Eng.) Trans. Biomed. Eng. 68 (5) (2021) 1638–1645.
- [28] Y. Zheng, X. Hu, Concurrent prediction of finger forces based on source separation and classification of neuron discharge information, Int. J. Neural Syst. 31 (6) (2021) 2150010.
- [29] F. Gao, S. Li, Z.-M. Li, M.L. Latash, V.M. Zatsiorsky, Matrix analyses of interaction among fingers in static force production tasks, Biol. Cybern. 89 (6) (2003) 407–414.
- [30] M.H. Schieber, C.E. Lang, K.T. Reilly, P. McNulty, A. Sirigu, Selective activation of human finger muscles after stroke or amputation, in: D. Sternad (Ed.), Progress in Motor Control, vol. 629, Springer US, 2009, pp. 559–575.
- [31] V.M. Zatsiorsky, Z.-M. Li, M.L. Latash, Enslaving effects in multi-finger force production, Exp. Brain Res. 131 (2000) 187–195.
- [32] X. Hu, N.L. Suresh, C. Xue, W.Z. Rymer, Extracting extensor digitorum communis activation patterns using high-density surface electromyography, Front. Physiol. 6 (2015) 279.
- [33] Y. Zheng, X. Hu, Interference removal from electromyography based on independent component analysis, IEEE Trans. Neural Syst. Rehabil. Eng. 27 (5) (2019) 887–894.
- [34] A. Hyvärinen, E. Oja, Independent component analysis: algorithms and applications, Neural Network. 13 (4–5) (2000) 4–5.
- [35] M. Chen, X. Zhang, Z. Lu, X. Li, P. Zhou, Two-source validation of progressive FastICA peel-off for automatic surface EMG decomposition in human first dorsal interosseous muscle, Int. J. Neural Syst. 28 (9) (2018) 09.
- [36] M. Chen, P. Zhou, A novel framework based on FastICA for high density surface EMG decomposition, IEEE Trans. Neural Syst. Rehabil. Eng. 24 (1) (2015) 1.
- [37] F. Negro, S. Muceli, A.M. Castronovo, A. Holobar, D. Farina, Multi-channel intramuscular and surface EMG decomposition by convolutive blind source separation, J. Neural. Eng. 13 (2) (2016) 2.
- [38] M. Muller, Dynamic time warping in information retrieval for music and motion, Dynamic Time Warping Information Retrieval for Music and Motion (2007) 69–84.
- [39] F. Nielsen, Hierarchical clustering, in: F. Nielsen (Ed.), Introduction to HPC with MPI for Data Science, Springer International Publishing, 2016, pp. 195–211.
- [40] Y. Zheng, X. Hu, Real-time isometric finger extension force estimation based on motor unit discharge information, J. Neural. Eng. 16 (6) (2019) 066006.
- [41] E.A. Clancy, N. Hogan, Probability density of the surface electromyogram and its relation to amplitude detectors, IEEE (Inst. Electr. Electron. Eng.) Trans. Biomed. Eng. 46 (6) (1999) 730–739.
- [42] J.E. Downey, L. Brane, R.A. Gaunt, E.C. Tyler-Kabara, M.L. Boninger, J. L. Collinger, Motor cortical activity changes during neuroprosthetic-controlled object interaction, Sci. Rep. 7 (1) (2017) 1.
- [43] P. Heo, G.M. Gu, S. Lee, K. Rhee, J. Kim, Current hand exoskeleton technologies for rehabilitation and assistive engineering, Int. J. Precis. Eng. Manuf. 13 (2012) 807–824.
- [44] C. Dai, X. Hu, Independent component analysis based algorithms for high-density electromyogram decomposition: experimental evaluation of upper extremity muscles, Comput. Biol. Med. 108 (2019) 42–48.
- [45] C. Dai, X. Hu, Independent component analysis based algorithms for high-density electromyogram decomposition: systematic evaluation through simulation, Comput. Biol. Med. 109 (2019) 171–181.
- [46] Y. Zheng, X. Hu, Adaptive real-time decomposition of electromyogram during sustained muscle activation: a simulation study, IEEE (Inst. Electr. Electron. Eng.) Trans. Biomed. Eng. 69 (2) (2021) 645–653.